Data Reduction of Room Tests for Zone Model Validation

MARC JANSSENS
National Forest Products Association
1250 Connecticut Avenue NW, Suite 200
Washington, DC 20036

HAO C. TRAN
USDA Forest Products Laboratory
One Gifford Pinchot Drive
Madison, WI 53705-2398

(Received April 16, 1992)
(Revised August 24, 1992)

ABSTRACT: Compartment fire zone models are based on many simplifying assumptions, in particular that gases stratify in two distinct layers. Because of these assumptions, certain model output is in a form unsuitable for direct comparison to measurements made in full-scale room tests. The experimental data must first be reduced and transformed to be compatible with the model output. In this article, new techniques are described to calculate neutral plane height, vent flow rates, uniform upper and lower layer temperature and interface height from measured temperature profiles. The new calculation procedures conserve mass in the room. The procedures were used for data reduction of a series of 8 gas burner calibration room tests. The results of one of the tests are discussed in detail as an illustrative example.

KEY WORDS: compartment fires, zone models, vent flow rates, temperature profiles.

INTRODUCTION

IN 1987, THE National Forest Products Association (NFoPA) initiated an

This paper was resented in part at the Interflam '90 Conference, University of Canterbury, England, /September 3-6,1990.

VOLUME 10 No. 6 0734-9041/92/06 0528–28 $06.00/0

extensive fire research program. The objective of the program is to develop a comprehensive mathematical model of fire growth in a compartment up to and beyond flashover and of the response of wood-based structural elements and assemblies to the resulting thermal exposure. A significant part of the program is focussed on a sub-model capable of predicting a wall or corner fire such as in ISO 9705 [1] or the draft ASTM room fire test [2]. This sub-model is hereafter referred to as CORNWALL.

In 1990, an extensive experimental program was completed at the U.S. Forest Products Laboratory (FPL). The experiments consisted of over 30 room tests and various fundamental full-scale fire experiments. This project was the subject of a joint study plan between NFoPA and FPL. Details of the room tests are reported elsewhere [3,4].

The objective of the full-scale experiments was to establish a data base for physical algorithm development and validation of the sub-model, CORNWALL, which is still under development. It is a two-layer zone model based on assumptions similar to those of other models of the same type, e.g., HARVARD/FIRST or FAST [5,6]. These assumptions however, result in the fact that the model only simulates an idealized and simplified variant of the real world,

As a consequence of the zone model assumptions, measurements made in full-scale room fire tests are usually not in the right form for model validation. Therefore, special data reduction and manipulation techniques must be used to transform the measurements into a format compatible with the model output. A number of such techniques are developed and described in this paper and their use is illustrated for one of the tests in the aforementioned experimental program.

EXPERIMENTS

The experimental program, set-up and some results are discussed in more detail elsewhere [3,4]. For completeness, some of this information is repeated below. The section on the experimental set-up describes details not reported earlier, but of particular importance for this paper.

Experimental Program

All full-scale tests were performed in a room according to the proposed ASTM room fire test method [2]. The experiments consisted of three distinct test series:

- *Calibration tests:* A series of 8 tests with the ASTM burner and non-combustible wall linings, i.e., either type X gypsum board or ceramic

fiber blanket. Four different burner programs in the range of 40 kW to 160 kW and two different burner locations were used.

- *Sensitivity study:* A series of 9 tests with either the back wall (wall tests) or the back wall and one of the side walls (corner tests) lined with Douglas fir plywood. The same parameters were varied as in the calibration test series.
- *Tests on five wood products:* 5 wood products were selected from an industry materials bank maintained at FPL. They were tested according to the two scenarios (wall and corner tests) and test conditions that were chosen on the basis of an analysis of the sensitivity study.

A number of tests were repeated leading to a total number of over 30 full-scale room fire tests.

Experimental Set-Up

All tests were conducted in a test rig conforming to the proposed ASTM room fire test method. The room measures 2.44 m wide × 3.66 m deep × 2.44 m high. There is a doorway in the front wall of 0.76 m wide by 2.03 m high. The ignition source was a propane sand burner measuring .305 m × .305 m, with the surface 0.305 m above the floor. For some of the tests (wall tests) the burner was put against the back wall at the center line. For all other tests (corner tests) the burner was located in one of the rear corners in contact with the back and a side wall.

Outside the room, all combustion products were collected in a hood. Flow rate, mole fraction of gas species ($O_2 CO_2$, CO and H_2O) and smoke obscuration were measured in the exhaust duct at a sufficient distance from the hood. Figure 1 shows additional instrumentation in the room. Some of this instrumentation is not prescribed by the ASTM proposal, but was included for the model validation techniques described in this paper. It includes:

- A thermocouple tree in the doorway (0.25 mm type K wire spaced at 0.1 m intervals between floor and soffit).
- A thermocouple tree in a quiescent zone inside the room (same size, spacing and heights as above).
- Transducers measuring static pressure difference across the front wall at four height levels: floor, 1.01 m, 1.52 m and soffit.

The temperature profile inside the room was measured in one of the front corners at 150 mm from both the front and side wall. In this corner, velocities are very small so that the surrounding zone may be

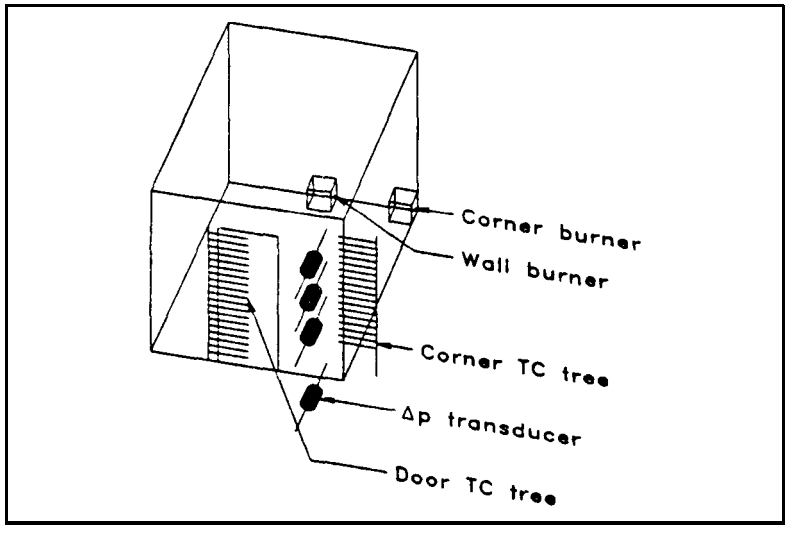

Figure 1. Additional instrumentation for mass flow calculations.

assumed to be quiescent. One of the leads of the pressure probes was also located in this zone in order to minimize the dynamic component of the pressure measured.

DATA REDUCTION FOR ZONE MODEL VALIDATION: THE PROBLEM

Room fire zone models are based on a number of assumptions. In reality, these assumptions are only partially valid. Therefore, full-scale data must be reduced and transformed into a format compatible with the zone model output in order to be useful for validation. In fact, given the model output variables, data reduction techniques as discussed in this paper also lead to guidelines on what measurements should be made and where they should be made.

For example, zone models assume that gases stratify in two distinct layers with uniform temperature and composition: an upper layer of hot gases underneath the ceiling and a lower layer of cool air. Figure 2 illustrates this idealized situation and also introduces some of the symbols we will use below. This is an acceptable approximation for most room fire situations. However, as illustrated by the dashed curve, real fire temperature profiles are smooth and the interface between the two layers is not sharp.

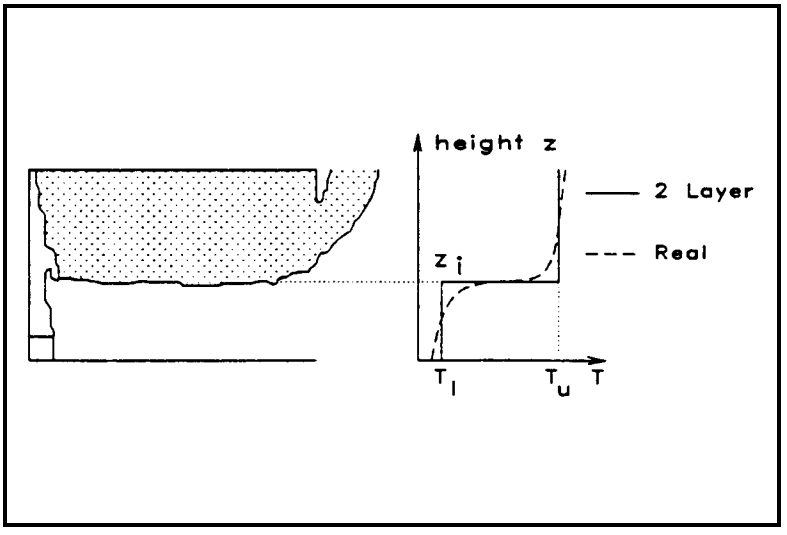

Figure 2. Real and two-layer temperature profiles.

In this paper we develop and discuss techniques to determine mass flow rates through the door, neutral plane height, uniform layer temperatures, and interface height from the measurements.

MASS FLOW RATES IN AND OUT OF THE ROOM

Several regimes can be distinguished over the course of a compartment fire as far as flow through the vent is concerned:

A. After ignition of the source, combustion products start to accumulate underneath the ceiling. As the smoke layer descends, cold air is pushed out of the vent. This effect is illustrated in Figure 3a.
B. At a certain time, the upper smoke layer reaches the soffit. However, the upper layer volume still increases at a rate faster than the entrainment of air into the fire. So, both upper layer gases and lower layer air leave the compartment as shown in Figure 3b.
C. Still later, a quasi-steady state establishes with cold air flowing into the compartment at the bottom of the vent and upper layer gases leaving the room at the top (Figure 3c).
D. If the fire grows beyond a certain limit (usually after flashover), the inflow of air into the compartment may no longer be controlled by the entrainment rate, but is restricted by the size of the ventilation

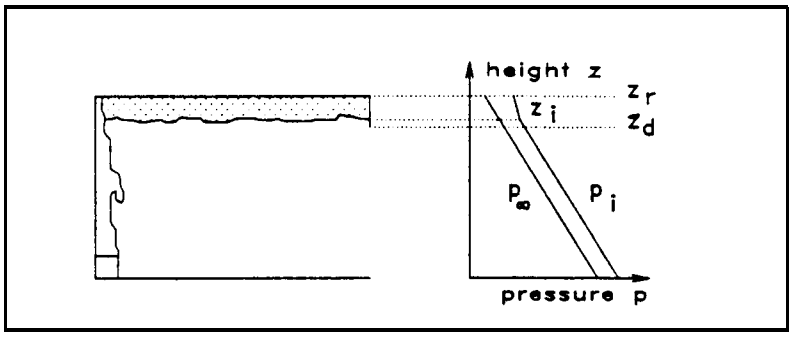

Figure 3a. Flow regime A.

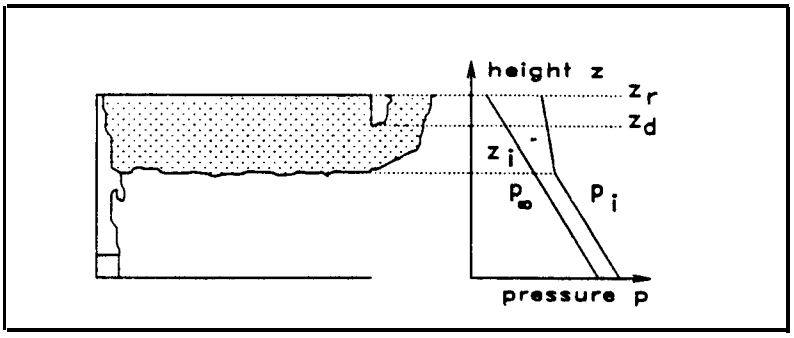

Figure 3b. Flow regime B.

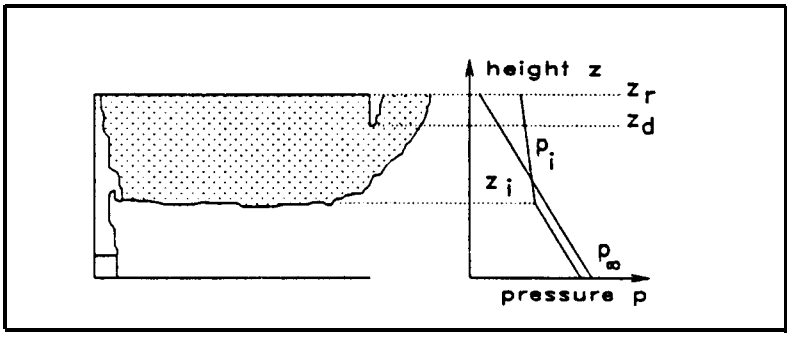

Figure 3c. Flow regime C.

opening. This "choking" or ventilation controlled regime was first discovered in 1958 by Kawagoe [7], who found air flow rates for this regime to be proportional to $A_d\sqrt{z_d}$.

E. Eventually, when the fire dies down, a regime develops which is the opposite from B.

In most compartment fires, regimes A and B prevail for only a short time (less than 30 seconds). Regime C is the most important regime prevailing during the remainder of the pre-flashover fire period and beyond. As our experimental fires were extinguished shortly after flashover (if occurring), discussion below applies to regimes A through C.

Assuming a uniform temperature inside the compartment, Kawagoe initially calculated vent flow rates in a fully-developed fire by treating the problem as that of flow through an orifice [7]. The same concept was followed by Thomas et al. in a two-layer model for gas flow through a roof vent [8]. Rockett expanded and generalized Kawagoe's and Thomas' expressions for fire induced gas flow in the early stages of an enclosure fire [9]. Extensive experimental work by Steckler et al. further validated the approach [10,11]. Steckler measured the velocity profile in the doorway for fifty-five steady state experiments using an array of bidirectional probes and thermocouples. Fire induced mass flow rates were calculated in two ways; by integrating the velocity profile, and via orifice flow calculations. Agreement was excellent. Steckler's work also resulted in the development of a practical experimental procedure to obtain vent flow rates without measuring velocity distributions [12].[1] Only temperature profiles and one static pressure difference measurement are needed. This procedure is described in a sub-section below.

Kawagoe used a flow coefficient of 0.7 in analogy with values used for pipe flow calculations [7]. Prahl and Emmons conducted salt water model experiments and obtained a value of 0.68 for sufficiently high Reynolds numbers [13]. An analysis of Steckler's data resulted in an average of 0.68 for inflow, and 0.73 for outflow [14]. Measured flow coefficients showed no significant dependence on fire strength, opening geometry, or fire location. Results from detailed numerical calculations of vent flow, modeled as an irrotational jet, were in reasonable agreement with the measurements.

General Equations

We developed a new technique to calculate fire induced flow from tem-

[1] Velocities in the doorway of room fires are quite low. The maximum is of the order of a few meters per second. Measurement of such low velocities is cumbersome and requires expensive pressure transducers.

perature profiles only. General equations for the vent flow rates as a function of temperature profiles are described in this sub-section. The equations are based on the orifice concept.

Flows in and out of the compartment are driven by pressure differences across the vent. Inside the compartment, velocities are negligible except locally in flames, plumes and wall jets. Thus, (static) pressure varies vertically only due to gravity. Idealized hydrostatic pressure profiles inside and outside the compartment for flow regimes A, B and C are shown in Figures 3a, 3b and 3C respectively. The velocity at height z is given according to Bernouilli's equation as

$$v(z) = \pm C \sqrt{2 \frac{|p_i(z) - p_\infty(z)|}{\varrho_d(z)}} \tag{1}$$

where

v = velocity ($m \cdot s^{-1}$)
C = orifice coefficient (--)
p_i = pressure inside the compartment (Pa)
p_∞ = pressure outside the compartment (Pa)
z = height above floor level (m), and
ϱ_d = density of gases in the doorway ($kg \cdot m^{-3}$)

For regime C, the height z_n at which there is no pressure difference (and no flow) between the compartment and the environment, is called the neutral plane. According to Reference [15], there is a maximum of one neutral plane for the case of a room connected to the outside (or a large reservoir). Hydrostatic pressure outside the compartment can be written as a function of height:

$$p_\infty(z) = p(z_n) + (z_n - z)\varrho_\infty g \tag{2}$$

where

ϱ_∞ = density of ambient air ($kg \cdot m^{-3}$), and
g = acceleration of gravity ($m \cdot s^{-2}$)

Hydrostatic pressure differences are very small (typically a few Pa) compared to the magnitude of the pressure itself, which is of the order of 10^5 Pa. Therefore, ϱ_∞ may be written as

$$\varrho_\infty = \frac{\varrho_{ref} T_{ref}}{T_\infty} = \frac{352.8}{T_\infty} \tag{3}$$

where

ϱ_{ref} = density of air at temperature T_{ref} and atmospheric pressure ($kg \cdot m^{-3}$)
T_{ref} = reference temperature (K)
T_∞ = temperature of ambient air (K)

With acceleration of gravity g = 9.81 $m \cdot s^{-2}$, Equation (2) then becomes

$$p_\infty(z) = p(z_n) + (z_n - z)\frac{3461}{T_\infty} \tag{4}$$

Inside the compartment, temperature is not constant with height. Thus, pressure as a function of height follows from

$$p_i(z) = p(z_n) + \int_z^{z_n} \frac{3461}{T_i(z')}\, dz' \tag{5}$$

Combining Equations (4) and (5) leads to the following expression for the pressure difference:

$$\Delta p(z) = 3461 \int_z^{z_n} \left(\frac{1}{T_i(z')} - \frac{1}{T_\infty} \right) dz' \tag{6}$$

The mass flow rate out of the compartment follows from integration of Equation (6):

$$\dot{m}_o = C_o W_d \int_{z_n}^{z_d} \varrho_d(z') v(z') dz' = C_o W_d \int_{z_n}^{z_d} \sqrt{2\varrho_d(z')\Delta p(z')}\, dz' \tag{7}$$

where

W_d = door width (m)
z_d = door height (m)

As the outflowing gases mainly consist of nitrogen, the density is not too different from that for air at the same temperature and pressure.

Substitution of Equation (6) and an expression analogous to Equation (3) for ϱ_d into Equation (7) yields

$$\dot{m}_o = 1563\, C_o W_d \int_{z_n}^{z_d} \left[\frac{1}{T_d(z')} \int_{z_n}^{z'} \left(\frac{1}{T_\infty} - \frac{1}{T_i(z'')} \right) dz'' \right]^{1/2} dz' \qquad (8)$$

Similarly, the inflow rate is equal to

$$\dot{m}_i = 1563\, C_i W_d \int_{0}^{z_n} \left[\frac{1}{T_d(z')} \int_{z'}^{z_n} \left(\frac{1}{T_\infty} - \frac{1}{T_i(z'')} \right) dz'' \right]^{1/2} dz' \qquad (9)$$

Note that a distinction is made between the orifice coefficient for inflow C_i and that for outflow C_o. This allows implementation of the recommendations in Reference [14].

z_n from Temperature Profiles and One Δp Measurement

Algorithms developed at NBS to reduce room fire data include a procedure to obtain z_n and mass flow rates through the vent [12]. These algorithms are referred to as RAPID. Equation (6) shows that Δp can be calculated as a function of height on the basis of the temperature profile measured inside the room if z_n is known. The NBS RAPID procedure requires measurement of Δp at one reference height z_{ref} in addition to the temperature profile inside the room. z_n can then be found by evaluating Equation (6) at z_{ref}.

$$\Delta p(z_{ref}) = 3461 \int_{z_{ref}}^{z_n} \left(\frac{1}{T_i(z')} - \frac{1}{T_\infty} \right) dz' \qquad (10)$$

The best reference height is at the soffit as pressure difference is usually the largest at this height. Once z_n is known, mass flow rates can be obtained according to Equations (8) and (9). This also requires the temperature profile in the doorway. Note that this method is also applicable to regimes A and B, although $\dot{m}_i$ in Equation (9) is zero and the integral in Equation 8 then goes from O to z_d.

z_n via Temperature Profiles Only

The RAPID procedure outlined in the previous section has some practical difficulties. $\Delta p\,(z_{ref})$ is on the order of a few Pa and is very difficult

to measure. Moreover, pressure data at such a low level are very noisy mainly due to turbulence. Another important drawback of the procedure is that it does not necessarily conserve mass. Therefore, a new procedure is developed here, based on temperature profiles only. The requirement for conservation of mass replaces Equation (10) as the equation for obtaining z_n. The mass balance equation has the following form:

$$\frac{dm_r}{dt} = \dot{m}_i + \dot{m}_b + \dot{m}_v - \dot{m}_o \tag{11}$$

where

m_r = mass accumulated inside the compartment (kg)
$\dot{m}_b$ = ignition source mass flow rate (kg·s^{-1})
$\dot{m}_v$ = release rate of fuel volatiles (kg·s^{-1})

$$\frac{dm_r}{dt} = 352.8\ W_r L \frac{d}{dt} \int_0^{z_r} \frac{dr'}{T_i(z')} \tag{12}$$

where

W_r = room width (m)
L = room length (m)
z_r = room height

The burner gas flow rate $\dot{m}_b$ is measured. $\dot{m}_v$ consists of water vapor and pyrolysis gases emerging from the walls. Both $\dot{m}_b$ and $\dot{m}_v$ are usually very small compared to the other terms in Equation (11) and can be neglected (although we did not). $\dot{m}_o$ and $\dot{m}_i$ are functions of z_n as indicated in Equations (8) and (9). Therefore, Equation (11) is a non-linear equation in z_n which can be solved iteratively.

Correction for Radiation Error

The temperature profiles in the quiescent corner and the doorway are measured with relatively fine thermocouples having a bead diameter of 0.9 mm. The temperature of the thermocouple beads is slightly different from that of the surrounding gas. The difference is due to the fact that the thermocouples absorb and emit radiation. This radiation error

may still be significant for the size of thermocouples used in the FPL room fire experiments. Calculation of the radiation error is very difficult. Only an approximate correction can be obtained. This estimate at least significantly reduces the radiation error.

The correction is based on the assumption that the incoming air is at ambient temperature near the floor, and that the lowest thermocouple in the doorway should therefore read ambient temperature. If during a test a higher temperature is measured, this is due to the fact that the thermocouple picks up radiation from the flames, the upper gas layer and heated walls. The corresponding radiative flux $\dot{q}_r''$ can be estimated from a heat balance of the thermocouple bead:

$$\alpha\left(\frac{1}{2}\dot{q}_r'' + \frac{1}{2}\sigma T_\infty^4\right) = h_m(T_{TC} - T_\infty) + \epsilon\sigma T_{TC}^4 \qquad (13)$$

where

α = absorptivity of the thermocouple bead (--)
h_m = convection coefficient ($W \cdot m^{-2} \cdot K^{-1}$)
T_{TC} = temperature of the thermocouple bead (K)
ϵ = emissivity of the thermocouple bead (--)

Over a distance of at least 100 mm from the hot junction, the thermocouple leads are horizontal, i.e., along an isotherm. Therefore, the heat balance does not include a conduction term. The thermocouple bead is approximately black so that $\alpha = \varepsilon = 1$. The convection coefficient h_m can be calculated from a correlation for forced convection over a single sphere [16]:

$$Nu_m = \frac{h_m D}{k} = 2 + (0.4\, Re^{1/2} + 0.06\, Re^{2/3}) Pr^{0.4} \qquad (14)$$

where

Nu_m = mean Nusselt number (--)
k = thermal conductivity of the surrounding gas ($W \cdot m^{-1} \cdot K^{-1}$)
D = diameter of the sphere (m)
Re = Reynolds number (vD/ν)
Pr = Prandtl number ($\nu\varrho c/k$)

Thermal conductivity k, viscosity ν, density ϱ and heat capacity c are for air and should be evaluated at the film temperature, i.e., the mean

of the thermocouple and the gas temperature. However, as the temperature difference between the fluid and the thermocouple is very small, the measured temperature was used. To obtain an estimate of the velocity at the lowest doorway thermocouple, the calculations outlined in the previous sub-sections are first performed without radiation error correction.

Once $\dot{q}_r''$ is known, gas temperature T_g at each doorway thermocouple below the netural plane is obtained from a heat balance similar to Equation (13):

$$\frac{1}{2}\dot{q}_r'' + \frac{1}{2}\sigma T_\infty^4 = h_m(T_{TC} - T_g) + \sigma T_{TC}^4 \qquad (15)$$

It is assumed that thermocouple junctions located above the neutral plane are exposed to $\dot{q}_r''$ on the fire side and to a plume at a temperature close to T_{TC} on the other side. The heat balance equation is then slightly different:

$$\frac{1}{2}\dot{q}_r'' = h_m(T_{TC} - T_g) + \frac{1}{2}\sigma T_{TC}^4 \qquad (16)$$

The thermocouples in the quiescent corner are located close to the walls. The wall temperature is not too different from T_{TC}. Moreover, the view factor between a hot junction and the fire is about the same for the doorway and corner thermocouples. Therefore, Equation (16) can also be used to estimate T_g in the corner. However, there is no forced flow in the corner and h_m must now be calculated from a correlation for free convection over a single sphere [17]:

$$Nu_m = 2 + 0.43\, Gr^{0.25} Pr^{0.25}, \qquad (17)$$

where

Gr = Grashof number $(gD^3 \Delta T/Tv^2)$

Sample Calculation

To illustrate the calculation procedures outlined above, a calibration room test (# 25R) was chosen as a sample case. The test was conducted with ceramic fiber blanket on the walls and with the burner in the wall configuration. The burner program was that of the original ASTM proposal, i.e., 40 kW for 30 seconds, 80 kW for the next 30 seconds, 120 kW

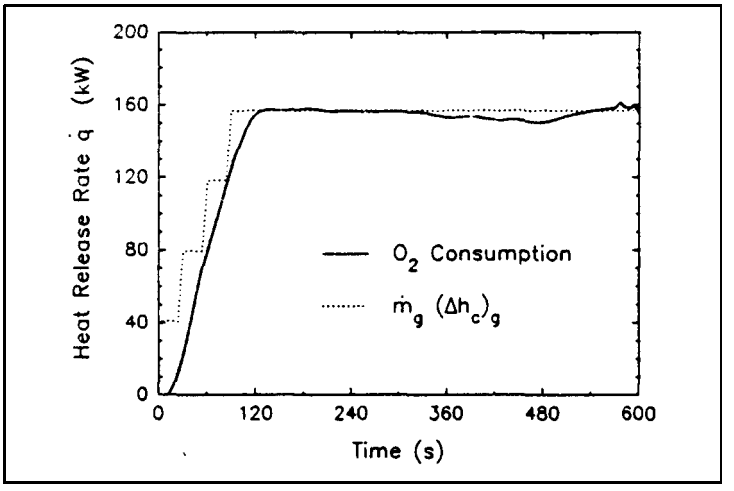

Figure 4. Measured and theoretical heat release rate for test # 25R.

for the following 30 seconds and finally 160 kW for the remaining 8.5 minutes of the test. Figure 4 compares the heat release rate calculated from oxygen consumption to the theoretical burner output, $\dot{m}_g \cdot (\Delta h_c)_g$.

A QuickBasic® program FPLMASS.BAS was written to perform the flow and radiation error correction calculations. All integrals were calculated using a trapezium rule. Linear interpolation was used to obtain temperature at heights in between the thermocouple locations. A value of 0.68 was chosen for C_i and C_o.

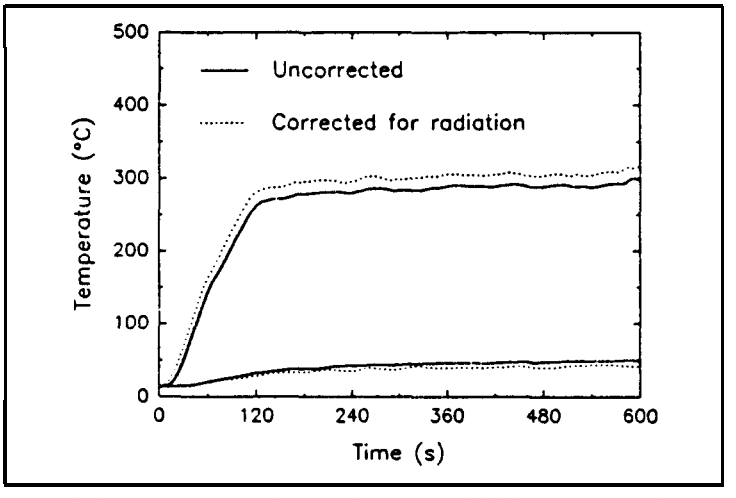

Figure 5. *Radiation error correction for* lowest and *highest corner thermocouple.*

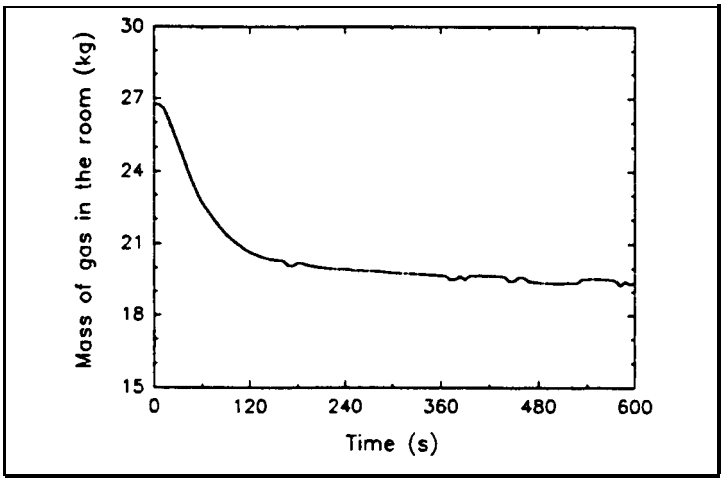

Figure 6. *Mass of gas accumulated in the room.*

Figure 5 indicates that the radiation error for test # 25R is between – 8°C and +20°C. Figure 6 shows the mass of gas in the room calculated from the corner profile with a time-integrated form of Equation (12). A five point numerical derivative results in the curve of the rate of change of the mass in Figure 7. Differential pressures measured at four elevations are shown in Figure 8. This figure indicates that the neutral plane height for most of the test duration is located slightly

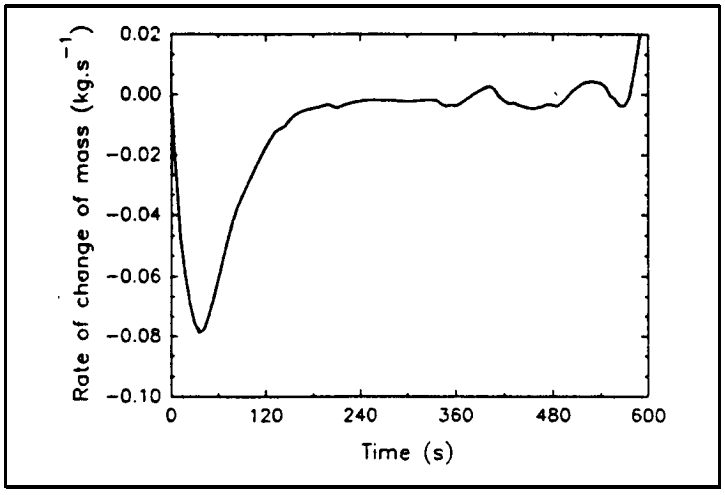

Figure 7. Rate *of change of mass in the room,*

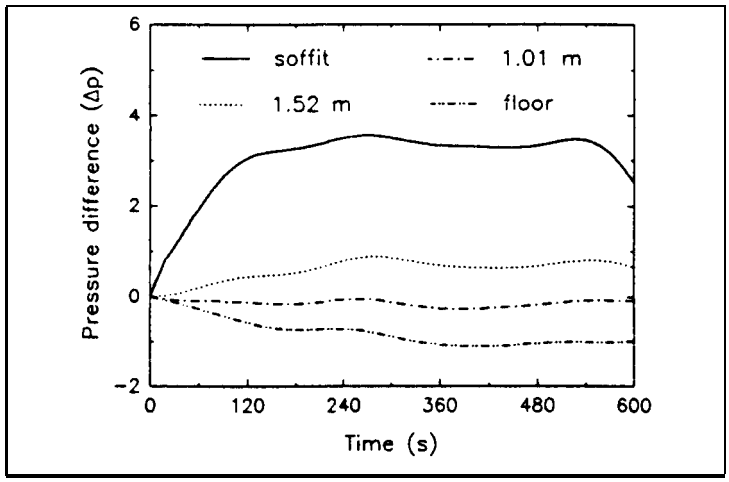

Figure 8. Δ p *across the front wall at four elevations.*

above the measuring point at 1.01 m. Figure 9 compares neutral plane height from interpolation of the measured Δp profile to the values calculated via the two procedures described in previous sub-sections. Agreement between the results obtained with the new mass balance technique and the interpolated data is reasonable. Neutral plane height calculated with the RAPID method using the largest and most accurate Δ_p(at the soffit) is considerably higher. Probably, this is pri-

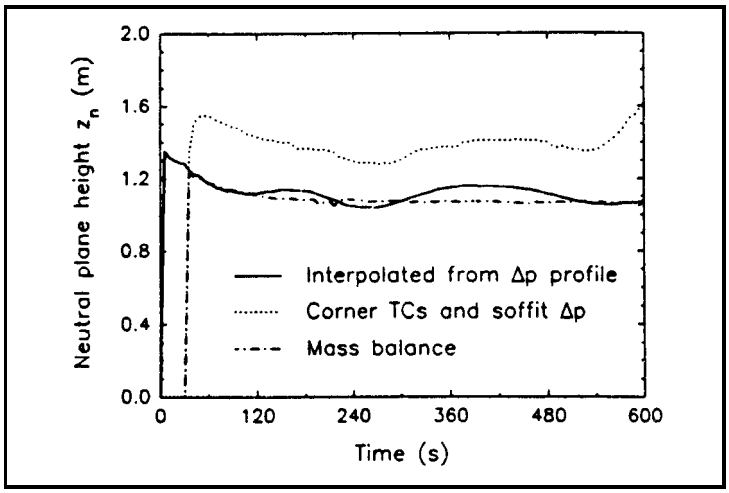

Figure 9. *Neutral plane height obtained with three different methods.*

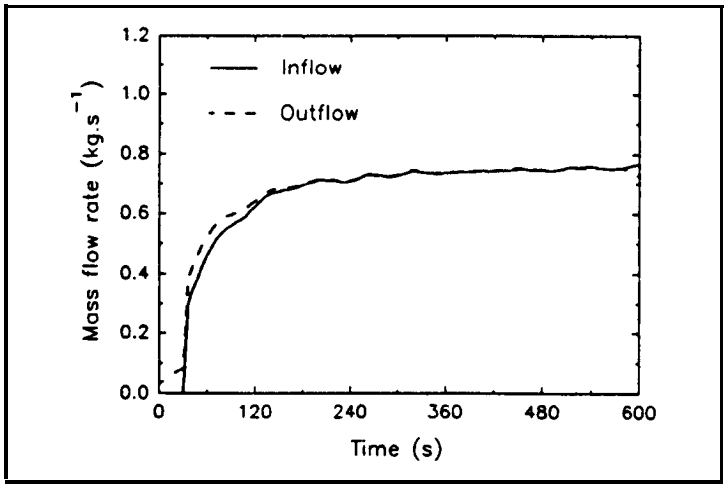

Figure 10. *Inflow and outflow via the mass balance technique.*

marily due to a systematic error in the pressure measurement at the soffit. Given the small magnitude of the pressure, considerable errors can hardly be avoided. The interpolation method is not so sensitive to such errors. This is because z_n is then determined from two pressure measurements and the errors partly cancel in the calculations.

The mass balance technique seems to have at least the same level of accuracy as the interpolation method. The technique also conserves mass (by definition), while it is obvious from Figure 9 that the RAPID procedure does not. Furthermore, since the need for expensive pressure transducers is eliminated, the mass balance technique is clearly the preferred method.

Figure 10 shows mass flow in and out of the compartment, calculated according to the mass balance technique. The difference between in. and $\dot{m}_i$ is due to the decrease of mass accumulated in the room because of heating. It can also be observed that the inflow rate is initially zero but becomes positive very shortly after the start of the test. Thus, flow regimes A and B do not last for more than 30 seconds.

LAYER TEMPERATURES AND INTERFACE HEIGHT

In this section techniques are developed and discussed to interpret the temperature profile measured inside the compartment in terms of a uniform upper layer temperature T_u, a uniform lower layer tempera-

ture T_l and an interface height z_i. Such techniques have been developed before. Cooper et al. suggested the so-called *N%* rule to determine z_i [18]. According to this rule, the interface at time *t* is at an elevation where the temperature rise over ambient equals N% of the maximum temperature rise of the top room thermocouple over the period up to *t*. Values of 10, 15 and 20% have been suggested for *N*. The 10% rule gave the best agreement with visual observations. Quintiere et al. obtained T_u from an arithmetic average of the upper thermocouple readings [19]. The following two integral identities were then used to compute T_l and z_i:

$$\int_0^{z_r} \frac{1}{T_r(z)}\,dz = \frac{z_r - z_i}{T_u} + \frac{z_i}{T_l} \tag{18}$$

$$\int_0^{z_r} T_r(z)dz = (z_r - z_i)T_u + z_i T_l \tag{19}$$

Equation (18) is a requirement for mass equivalency. Equation (19) describes a mathematical averaging procedure, but has no physical meaning. Emmons proposed to use the reading of the bottom thermocouple for T_l, to take z_i as the elevation where the slope of the temperature profile goes through a maximum and then to determine T_u from mass equivalency [Equation (18)] [20]. Unfortunately, none of the existing techniques ensure that the two-layer profile leads to identical vent flow rates as measured. To eliminate this potential problem, a new procedure was developed. The improved procedure is outlined in the next sub-section.

General Equations

For the case of a fire room connected to the environment through a single opening, at most one neutral plane can be located between the floor and the soffit [15]. The gases inside the room expand in the initial stages of a test. Inside pressure is higher than ambient over the full height of the ventilation opening. There is no inflow and the elevation of the neutral plane is below floor level, so that $z_i > z_n$. At some instant, the expansion no longer compensates for the rate of entrainment into the fire. The neutral plane rises above floor level and ambient air is drawn into the compartment. The neutral plane height is continuously adjusted so that there is conservation of mass. The elevation of the interface between the layers is controlled by the fact that the rate

of entrainment into the fire over height z_i is more or less equal to $\dot{m}_i$.[2] Depending on the size of the fire, z_i may be higher or lower than z_n. For small fires (such as test # 25R), the interface is located above the neutral plane. For high intensity fires the opposite may be the case.

The procedure to determine T_l, T_u and z_i developed in this section is primarily based on the requirement that vent flow rates calculated with the two-layer profile should be identical to those obtained with the measured temperature profile. The latter is determined in the process of calculating z_n via the mass balance technique. With a two-layer profile, the integrations in Equations (8) and (9) can be performed analytically. Non-linear expressions for $\dot{m}_i$ and $\dot{m}_o$ as a function of T_l, T_u and z_i are obtained as a result. These equations are rather complex. To simplify the notation, some new symbols are defined first:

$$\Theta_{\infty l} \equiv \frac{1}{T_\infty}\left(\frac{1}{T_\infty} - \frac{1}{T_l}\right) \tag{20}$$

$$\Theta_{\infty u} \equiv \frac{1}{T_\infty}\left(\frac{1}{T_\infty} - \frac{1}{T_u}\right) \tag{21}$$

$$\Theta_{ll} \equiv \frac{1}{T_l}\left(\frac{1}{T_\infty} - \frac{1}{T_l}\right) \tag{22}$$

$$\Theta_{ul} \equiv \frac{1}{T_u}\left(\frac{1}{T_\infty} - \frac{1}{T_l}\right) \tag{23}$$

$$\Theta_{uu} \equiv \frac{1}{T_u}\left(\frac{1}{T_\infty} - \frac{1}{T_u}\right) \tag{24}$$

$$\gamma_i \equiv 1042\, C_i W_d \tag{25}$$

$$\gamma_o \equiv 1042\, C_o W_d \tag{26}$$

When calculating the integrals, a distinction has to be made between two cases, depending on whether $z_i \leq z_n$ or $z_i \geq z_n$.

Case 1: $z_i \leq z_n$

The two-layer temperature profiles inside the room and in the doorway can be expressed as piece-wise constant functions of height *z:*

[2] There may be a significant difference due to mixing at the door and due to wall jets [21], which at the present time is ignored.

Substitution of Equation (27) in Equation (9) and integration results in

$$\dot{m}_i = \frac{\gamma_i}{\Theta_{\infty l}} \{[\Theta_{\infty l} z_i + \Theta_{\infty u}(z_n - z_i)]^{3/2} + (\Theta_{\infty u}^{1/2}\Theta_{\infty l} - \Theta_{\infty u}^{3/2})(z_n - z_i)^{3/2}\} \quad (28)$$

T_l should always be higher than T_∞, so that there is no problem in the evaluation of Equation (28). In the limiting case of $T_l = T_\infty$, application of l'Hôpital's rule leads to

$$\dot{m}_i = \gamma_i \Theta_{\infty u}^{1/2}(z_n - z_i)^{1/2}\left(z_n + \frac{z_i}{2}\right) \quad (29)$$

An equation for the outflow rate is obtained in a similar way as for the inflow:

$$\dot{m}_o = \gamma_o \Theta_{uu}^{1/2}(z_d - z_n)^{3/2} \quad (30)$$

Using z_n and $\dot{m}_o$ obtained with the mass balance technique, T_u is the

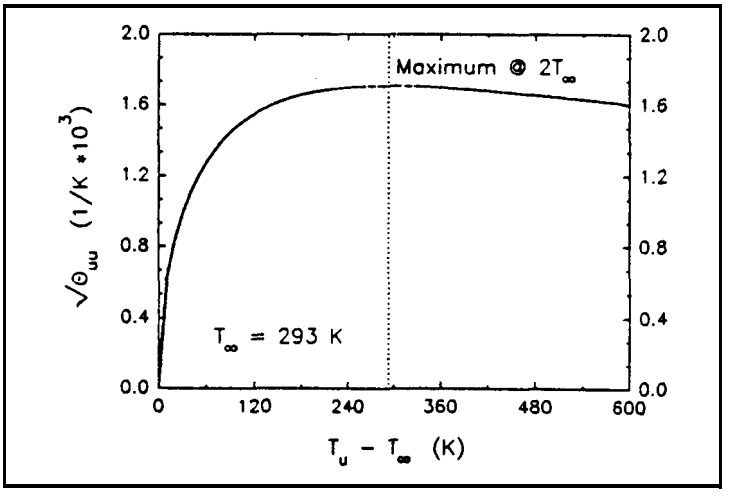

Figure 11. *Variation of* $\sqrt{\Theta_{uu}}$ *as a function of* T_u.

only unknown in Equation (30). Unfortunately, as illustrated in Figure 11, the right hand side of Equation (30) is more or less constant for $T_u > 200°C$. Thus, at sufficiently high T_u a small difference in $\dot{m}_o$ results in a very large change in the corresponding upper layer gas temperature. Worse, due to the error in the calculated $\dot{m}_o$, Equation (30) may not even have a solution! Clearly, using Equation (30) to determine T_u is not a good idea. To circumvent the problem, T_u is estimated from the average of all temperatures that are within 5% of the maximum temperature measured in the quiescent corner. There is no justification for this, other than that it is convenient and seems to give reasonable results.

A possible approach for obtaining the remaining unknowns T_l and z_i consists of solving the set of two non-linear algebraic Equations (18) and (28). Note that the requirement for mass equivalency, Equation (18), automatically ensures that the rate of change of mass in the room from the calculated two-layer profile is identical to that obtained from Equation (11). A powerful numerical solver based on Powell's method was chosen for some preliminary calculations [22]. This solver does not require the user to specify the Jacobian, but uses a finite-difference approximation to estimate the partial derivatives. Unfortunately, the resulting values for z_i were considerably lower than those estimated visually from the measured temperature profiles.

To obtain better agreement between measured and two-layer profiles, an alternative procedure was developed. It consists of the following steps:

- Estimate T_u from an average of upper layer thermocouple readings.
- Obtain z_i from the inflection point of the measured temperature profile.
- Calculate T_l from mass equivalency [Equation (18)].
- Compute a new value for z_n from the mass balance Equation (11), using Equations (28) and (30) for $\dot{m}_i$ and $\dot{m}_o$ respectively. Once z_n is found, the vent flow rates follow from the same equations, Equations (28) and (30).

The alternative approach is the preferred. It yields two-layer temperature profiles that are in qualitative agreement with the measured profiles. The adjusted values for z_n, $\dot{m}_i$ and $\dot{m}_o$ are within 10% of those obtained with the mass balance technique outlined in the previous section. The two-layer variant of the mass balance technique is referred to below as the *adjusted mass balance* technique.

Case 2: $Z_i \geq Z_n$

The two-layer temperature profiles inside the room and in the doorway can again be expressed as piece-wise constant functions of height:

$$\begin{aligned} 0 \leq z_n: T_d(z) &= T_\infty \qquad T_r(z) = T_l \\ z_n < z \leq z_i: T_d(z) &= T_l \qquad T_r(z) = T_l \\ z_i < z \leq z_d: T_d(z) &= T_u \qquad T_r(z) = T_u \end{aligned} \tag{31}$$

Substitution of Equation (31) in Equation (9) and integration results in

$$\dot{m}_i = \gamma_i \Theta_{\infty l}^{1/2} z_n^{3/2} \tag{32}$$

An equation for the outflow rate follows in a similar way:

$$\dot{m}_o = \frac{\gamma_o}{\Theta_{uu}} \{[\Theta_{uu}(z_d - z_i) + \Theta_{ul}(z_i - z_n)]^{3/2} + (\Theta_{ll}^{1/2}\Theta_{uu} - \Theta_{ul}^{3/2})(z_i - z_n)^{3/2}\} \tag{33}$$

For similar reasons as mentioned for Case 1, the adjusted mass balance technique is recommended. It consists of the same steps as listed above, except that Equations (32) and (33) replace Equations (28) and (30) respectively.

Sample Calculation

Again, test # 25R is taken as an example. The heat release rate in this test is fairly low so that the interface is located above the neutral plane throughout the test. Thus, the equations for Case 2 outlined in the previous sub-section are applicable. Figure 12 indicates that z_i on the average is about 0.5 m higher than the adjusted z_n. The latter is located about 0.05 m below z_n obtained with the original mass balance technique.

Note that in the initial stages of the fire (flow regimes A and B), z_n is below floor level and $\dot{m}_i$ is zero. However, the adjusted mass balance technique can still be used to find z_i, T_l and T_u. The calculated layer temperatures for test # 25R are shown in Figure 13. The two-layer and measured room temperature profiles at the end of the test are compared in Figure 14. This gives a fairly good idea of how well the idealized profile represents reality.

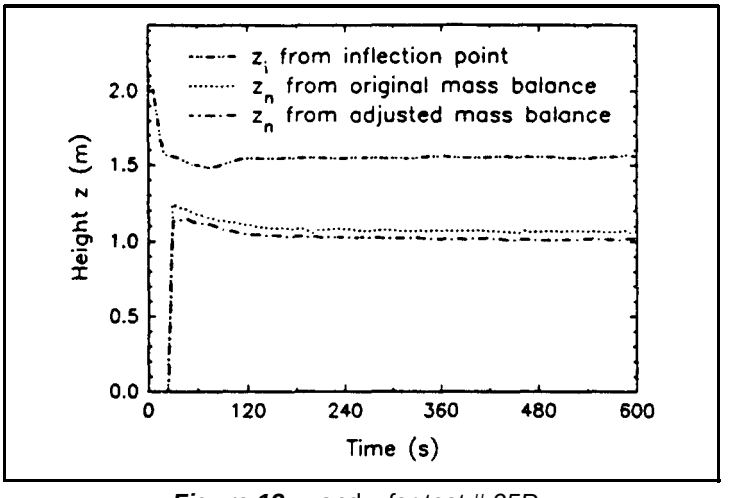

Figure 12. z_n and z_i *for test # 25R.*

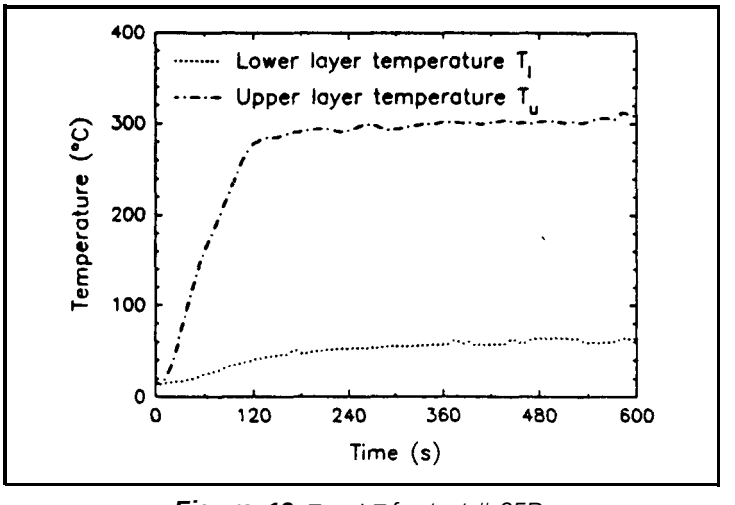

Figure 13. T_u and T_l *for test # 25R.*

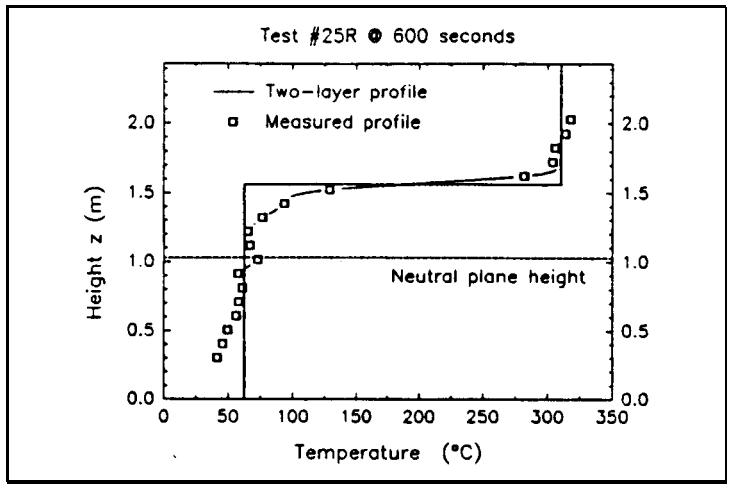

Figure 14. *Two-layer and measured room temperature profiles at 600 seconds in test # 25R.*

CONCLUSIONS

In this article, techniques are described to calculate vent flow rates, neutral plane height, interface height and uniform layer temperatures from measured temperature profiles alone. With respect to mass flow rates and neutral plane height, the suggested procedure leads to smoother and perhaps more accurate results than an existing technique which also requires the measurement of static pressure differences at one height in addition to temperature profiles. Interpretation of measured temperature profiles in terms of idealized two-layer profiles requires a minor adjustment to the calculated neutral plane height (and consequently the vent flow rates), to ensure conservation of mass with the two-layer temperature profiles. Application to one calibration test indicates the techniques give acceptable results. Application to other tests in the experimental program and comparison with model results are needed before the final statement can be made about the validity and accuracy of the proposed method.

NOMENCLATURE

A cross-sectional area (m^2)
C orifice coefficient (--)
c heat capacity ($J \cdot kg^{-1} \cdot K^{-1}$)

D thermocouple bead diameter (m)
g gravitational constant (9.81 $m \cdot s^{-2}$)
Gr Grashof number (--)
h convection coefficient ($W \cdot m^{-2} \cdot K^{-1}$)
k thermal conductivity ($W \cdot m^{-1} \cdot K^{-1}$)
L room length (m)
m mass (kg)
$\dot{m}$ mass flow rate ($kg \cdot s^{-1}$)
Nu Nusselt number (--)
Pr Prandtl number (--)
p pressure (Pa)
$\dot{q}$ rate of heat release (kW)
$\dot{q}''$ heat flux ($kW \cdot m^{-2}$)
Re Reynolds number (--)
T temperature (K)
v velocity ($m \cdot s^{-1}$)
W width (m)
z height above floor (m)
z', z'' integration variables

Greek Symbols

α thermocouple absorptivity (--)
γ symbol used in vent flow equations
Δ difference
Δh_c net heat of combustion of the burner gas ($kJ \cdot kG^{-1}$)
ϵ emissivity (--)
Θ symbol used in vent flow equations
ν kinematic viscosity ($m^2 \cdot s^{-1}$)
ϱ density ($kg \cdot m^{-3}$)
σ Boltzmann constant ($5.67 \cdot 10^{-11}\ kW \cdot m^{-2} \cdot K^{-4}$)

Subscripts

b burner
d doorway, soffit
g burner gas, gas
i inside of room, inflow, layer interface
l lower layer
m mean
n neutral plane
o outflow

$_r$ room
ref reference, radiation
TC thermocouple
$_u$ upper layer
$_v$ volatiles
$_\infty$ ambient

REFERENCES

1. International Standards Organization. In press. "ISO 9705: Full-Scale Room Fire Test," Geneva: ISO.
2. American Society for Testing and Materials. 1983. "Proposed Method for Room Fire Test of Wall and Ceiling Materials and Assemblies," *ASTM Annual Book of Standards,* 04.07:958–978.
3. Tran, H. and M. Janssens. 1989. "Room Fire Test for Fire Growth Modeling–A Sensitivity Study," *Journal of Fire Sciences,* 7:217–236.
4. Tran, H. and M. Janssens. 1991. "Wall and Corner Fire Tests on Selected Wood Products," *Journal of Fire Sciences,* 9:106–124.
5. Mitler, H. 1978. "The Physical Basis for the Harvard Computer Fire Code," Home Fire Project Technical Report No. 34, Cambridge, MA: Harvard University.
6. Jones, W. 1985. "A Multicompartment Model for the Spread of Fire, Smoke and Toxic Gases," *Fire Safety Journal,* 9:55–79.
7. Kawagoe, K. 1958. "Fire Behaviour in Rooms," Report of the Building Research Institute No. 27., Tokyo, Japan: Ministry of Construction.
8. Thomas, P., P. Hinkley, C. Theobald and D. Simms. 1963. "Investigations into the Flow of Hot Gases in Roof Venting," Fire Research Technical Paper No. 7, London, UK: Ministry of Technology.
9. Rockett, J. 1976. "Fire Induced Gas Flow in an Enclosure," *Combustion Science and Technology,* 12:165–175.
10. Steckler, K., J. Quintiere and W. Rinkinen. 1982. "Flow Induced by Fire in a Compartment," NBS-IR 82-2520, Gaithersburg, MD: National Bureau of Standards.
11. Nakaya, I., T. Tanaka, M. Yoshida and K. Steckler. 1986. "Doorway Flow Induced by a Propane Fire," *Fire Safety Journal,* 10:185–195.
12. Breese, J. and R. Peacock. 1986. "A User's Guide for RAPID, Reduction Algorithms for the Presentation of Incremental Fire Data," Special Publication 772, Gaithersburg, MD: National Bureau of Standards.
13. Prahl, J. and H. Emmons. 1975. "Fire Induced Flow through Openings," *Combustion and Flame,* 25:369–385.
14. Steckler, K., H. Baum and J. Quintiere. 1984. "Fire Induced Flows through Room Openings-Flow Coefficients," *Twentieth Symposium (International) on Combustion, Pittsburgh, PA: The Combustion Institute,* pp. 1591–1600.
15. Jones, W. and R. Peacock. 1989. *Technical Reference Guide to FAST 18.*

Technical Note 1262, Gaithersburg, MD: National Institute of Standards and Technology.

16. Whitaker, S. 1972. "Forced Convection Heat Transfer Calculations for Flow in Pipes, Past Flat Plates, Single Cylinders, and for Flow in Packed Beds and Tube Bundles," *AICHE J.,* 18:261–371.
17. Yuge, T. 1960. "Experiments on Heat Transfer from Spheres, Including Combined Natural and Free Convection," *J. Heat Transfer,* 82C:214–220.
18. Cooper, L., M. Harkleroad, J. Quintiere and W. Rinkinen. 1982. "An Experimental Study of Upper Hot Layer Stratification in Full-Scale Multiroom Scenarios," *J. Heat Transfer,* 104:741–749.
19. Quintiere, J., K. Steckler and D. Corley. 1984. "An Assessment of Fire Induced Flows in Compartments," *Fire Science and Technology,* 4:1–14.
20. Emmons, H. 1989. "Vent Flows," In the *SFPE Handbook for Fire Protection Engineering,* Ph. DiNenno, ed., Boston, MA: Society of Fire Protection Engineers, Part 1, pp. 130–137.
21. Quintiere, J. 1984. "A Perspective on Compartment Fire Growth," *Combustion Science and Technology,"* 39:11–54.
22. Powell, M. 1979. "A Hybrid Method for Nonlinear Equations," in *Numerical Methods for Nonlinear Algebraic Equations,* P. Rabinowitz, ed., New York: Gordon and Breach.

BIOGRAPHIES

Marc Janssens

Marc Janssens is Manager Fire Technology of the American Wood Council of the National Forest Products Association (NFoPA). He has an MS and Ph.D. in Mechanical Engineering from the University of Ghent in Belgium, Between 1980 and 1987, he conducted research on full-scale and bench-scale fire testing and fire modeling at Ghent. He built the first Cone Calorimeter outside NIST in 1986. Since 1984 he is convener of ISO/TC92/SC1/WG5, developing the Cone Calorimeter into an International Standard. In August of 1987 he moved to the United States and continued his research for NFoPA at NIST. In May of 1990, he was transferred to the office of NFoPA in Washington, DC where he assumes his current position.

Hao Tran

Hao Tran is a Research Scientist at the U.S. Forest Products Laboratory (FPL) in Madison, Wisconsin. He has a BSc and MS in Wood Science and Technology, and a Ph.D. in Agricultural and Environmental

Chemistry from the University of California at Berkeley. Since 1986, he has been working at FPL in the Fire Safety of Wood Products Research Work Unit. In this capacity, he does research on several aspects of fire growth, including ignition, flame spread, heat and smoke release rate of wood products.

Printed on recycled paper